Quaternary Science Reviews 343 (2024) 108939

Contents lists available at ScienceDirect

Quaternary Science Reviews

journal homepage: www.elsevier.com/locate/quascirev

Arvicolinae rodents of Galería de las Estatuas (Sierra de Atapuerca, Burgos) and insights into MIS 5- to −4 climatic conditions in Northern Iberia

M.P. Alfaro-Ibáñez [a,*], G. Cuenca-Bescós [a], A. Gómez-Olivencia [b,c,d], M. Demuro [e], L.J. Arnold [e], J.L. Arsuaga [f,d]

[a] Aragosaurus-IUCA, Ciencias de la Tierra, Facultad de Ciencias, Universidad de Zaragoza, Pedro Cerbuna, 12, E-50009, Zaragoza, Spain
[b] Departamento de Geología, Facultad de Ciencia y Tecnología, Universidad del País Vasco/Euskal Herriko Unibertsitatea (UPV/EHU), Barrio Sarriena s/n, 48940, Leioa, Spain
[c] Sociedad de Ciencias Aranzadi, Zorroagagaina 11, 20014, Donostia-San Sebastián, Spain
[d] Centro UCM-ISCIII Investigación sobre Evolución y Comportamiento Humanos, Avda. Monforte de Lemos 5, (Pabellón 14), 28029, Madrid, Spain
[e] School of Physics, Chemistry and Earth Sciences, Environment Institute, Institute for Photonics and Advanced Sensing (IPAS), University of Adelaide, North Terrace Campus, 5005, Adelaide, SA, Australia
[f] Departamento de Geodinámica, Estratigrafía y Paleontología, Facultad de Ciencias Geológicas, Universidad Complutense de Madrid, c/ José Antonio Novais, 12, Ciudad Universitaria, 28040, Madrid, Spain

ARTICLE INFO

Keywords:
Paleoecology
Pleistocene
Western Europe
Single-grain OSL dating
Small mammals

ABSTRACT

Well-dated Middle Palaeolithic sequences that lie beyond the limit of radiocarbon dating (i.e., >50,000 years ago) are critical for understanding the long-term palaeoecological changes that took place during Neandertal occupation of Europe and the Iberian Peninsula. Among the two pits excavated in Galería de las Estatuas site, GE (Sierra de Atapuerca, Burgos, Spain) represents such sequence, having been previously dated using a combination of single-grain optically stimulated luminescence (OSL) and U-series. This site is one of the few across Eurasia to have yielded both Neandertal remains and genetic evidence of Neandertal population replacements during marine isotope stage (MIS) 5 to the beginning of MIS 4 (120,000 to 70,000 years ago). Understanding the prevailing climatic and environmental conditions during the period of Neandertal occupation is therefore of great importance. Small mammal remains are one of the best proxies to interpret past environmental and climatic changes, and among these, the Arvicolinae species (Cricetidae, Rodentia) are particularly useful.

Here we provide a revision of the small mammal associations at both Galería de las Estatuas pits undertaking detailed study of Arvicolinae species composition in both excavation pits. Additionally, we present new single-grain OSL dating results to refine the existing chronostratigraphic framework and better contextualise the past climatic changes inferred from the small mammal record. Our results indicate that the lower levels were formed in cold-temperate conditions, with a predominance of an open landscape and Atlantic-type climatic regime. Progressively upward through the sequences, we observe warmer and more humid conditions, with a stronger Mediterranean climate regime and increased development of forest areas, although still with a predominance of open meadows. Finally, both sedimentary sequences seem to end with a deterioration of these climatic conditions, and show a drier environment, dominated by open landscapes and a return to an Atlantic climatic regime. We conclude that at least two marked climatic changes can be identified at each pit (GE-I and GE-II), from MIS 5.4 through to the beginning of MIS 4, by studying the small mammal record together with OSL dating.

1. Introduction

Analysis of small mammal associations in the fossil record is an important tool for Quaternary studies, including reconstructing past climates, changes in biodiversity and the environment, among others. This is partly due to the high evolutionary rate of some small mammal species and genera, as is the case for certain rodent species (Cuenca-Bescós and Morcillo-Amo, 2022). Additionally, the capacity of small mammals to specialize in various environments and habitats makes them particularly useful for studies of biostratigraphy and

* Corresponding author.
E-mail address: alfaromp@unizar.es (M.P. Alfaro-Ibáñez).

https://doi.org/10.1016/j.quascirev.2024.108939
Received 2 May 2024; Received in revised form 24 June 2024; Accepted 29 August 2024
Available online 1 September 2024

biochronology. Their abundance and specific diversity are strongly affected by climatic variations (e.g., Blois et al., 2010; Cuenca-Bescós et al., 2008; López-García et al., 2021), and therefore they are important proxies for past climatic changes.

Scientific studies of small mammal records have previously been used at various paleontological and archaeological sites from the Iberian Peninsula, including those of the Sierra de Atapuerca (from now on referred as Atapuerca), to examine biochronology and biostratigraphy relationships or infer past climatic changes (Arsuaga et al., 2017; Bennàsar Serra et al., 2016; Cuenca-Bescós et al., 2010, 2011; Galán et al., 2022; López-García et al., 2010; Bañuls-Cardona et al., 2017). The study of the Arvicolinae (Cricetidae, Rodentia) species has been of particular importance in small mammal studies because they exhibit some of the largest and most rapid diversification processes of the Pleistocene, as well as significant variability in their habitat and climate ranges (Chaline et al., 1999; Van der Meulen, 1973).

Among the Atapuerca sites, Galería de las Estatuas (GE) stands out as representing the first site within the karst system to contain (i) an archeo-paleontological record from the Upper Pleistocene with detectable ecological changes and Mousterian lithic records (Arsuaga et al., 2017); (ii) Neandertal fossil remains (Pablos et al., 2019); (iii) a sedimentary record containing Neandertal ancient DNA (Vernot et al.,

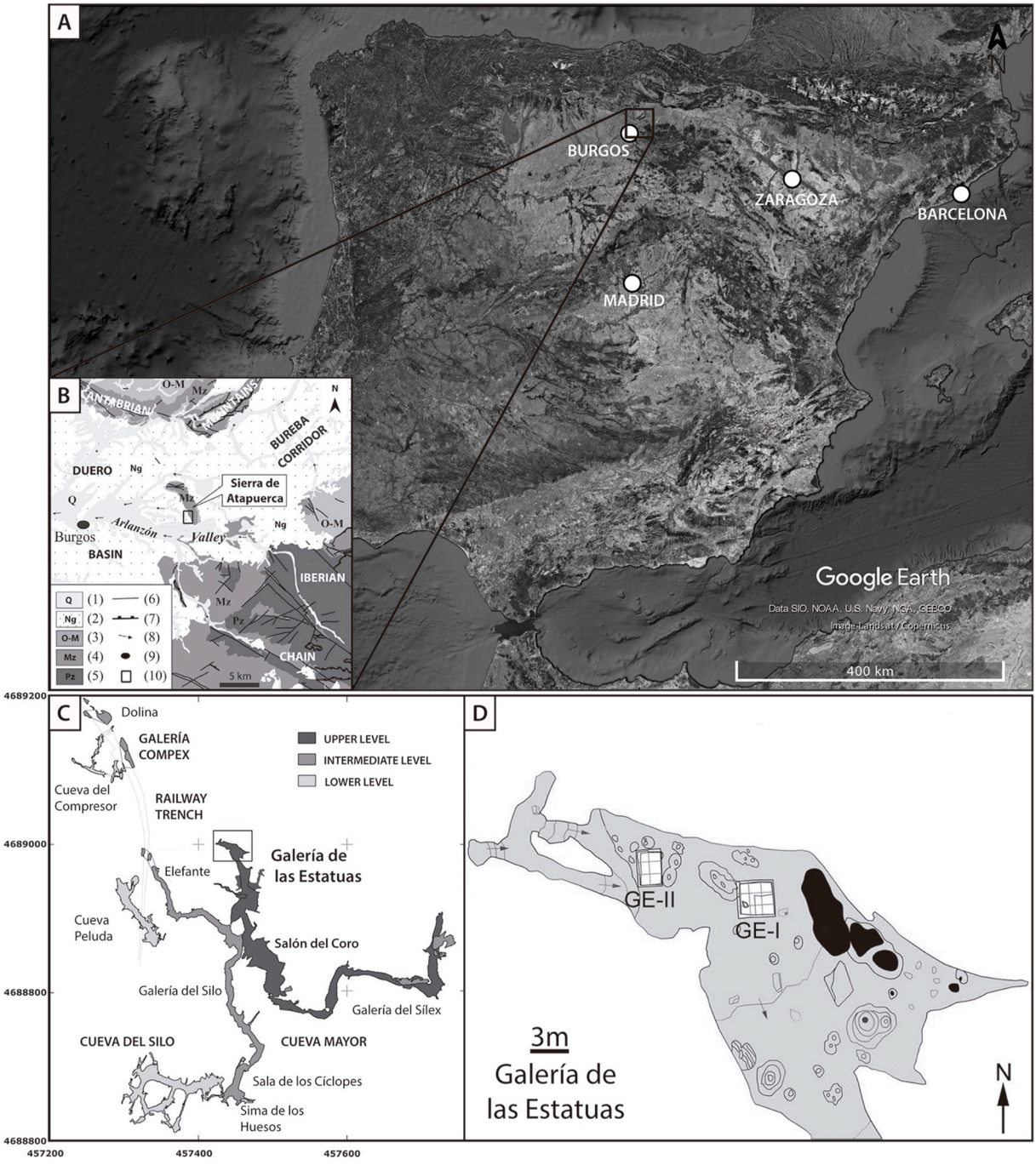

Fig. 1. Geographic **(A)** and geological **(B)** location of the Atapuerca sites (modified from Ortega et al., 2013). Location of the pits of Galería de las Estatuas (GE) site within the Cueva Mayor-Cueva del Silo cave complex **(C)** (topography map, in UTM coordinates, modified from Ortega, 2009), and distribution of the two excavated pits **(D)** (modified from Arsuaga et al., 2017). Legend from **(B)**: (1) Quaternary; (2) Neogene; (3) Oligocene/Lower Miocene; (4) Mesozoic; (5) Palaeozoic; (6) fault; (7) thrust; (8) drain age direction; (9) Burgos; (10) Sierra de Atapuerca.

2021); and (iv) a sedimentary sequence dated to marine isotope stages (MIS) 5–4 (Demuro et al., 2019; Moreno et al., 2022). The study of the Galería de las Estatuas rodent record is indispensable for obtaining further environmental, climatic and biochronological information for this globally significant site.

The aims of this paper are to (i) present a detailed taxonomical study of the Arvicolinae record at GE and complement existing information on the climatic and environmental changes that took place during the formation of the site, and (ii) present new single-grain optically stimulated luminescence (OSL) dating results from the fossil-bearing sedimentary layers of excavation pit GE-II. This holistic approach is then used to improve the chronological frameworks and paleoclimatic interpretations across pits GE-I and GE-II.

2. The Sierra de Atapuerca and Galería de las Estatuas site

2.1. Geographical and geological location

The Atapuerca archeo-paleontological complex comprises some of the most important sites in Europe, due to their unique archaeological and paleontological discoveries (e.g. Arsuaga et al., 2014, 2017; Carbonell et al., 2008; Cuenca-Bescós et al., 2011). The almost continuous record extends back from the Early Pleistocene to Holocene (e.g., Arnold et al., 2014; Berger et al., 2008; Demuro et al., 2019, 2022; Duval et al., 2022). Atapuerca is situated along the Bureba corridor, which connects two river basins of the Iberian Peninsula, the Ebro and the Duero basins. It is located between two major mountain systems, the Iberian system, and the Cantabrian Mountain range (Fig. 1A and B) (Arsuaga et al., 2014, 2015; Bermúdez de Castro et al., 1997; Carbonell et al., 2008; Ortega, 2009).

GE is located in the upper level of the Cueva Mayor-Cueva del Silo multilevel karstic complex of Atapuerca, (Fig. 1C and D). The site formed within an ancient entrance of the system, but at present is closed to the exterior (Arsuaga et al., 2017; Ortega, 2009).

2.2. The GE excavation pits and stratigraphic levels

The excavations at the Galería de las Estatuas site began inside the cave in 2008, while excavations in the exterior of the cave, at the location corresponding to the suspected palaeo-entrance began in 2020. Two pits, named GE-I and GE-II, are being excavated at Galería de las Estatuas interior and both display siliciclastic deposits overlain by stalagmitic flowstone (Fig. 1D). The first pit that was excavated, GE-I, shows 5 lithostratigraphic units (LU) identified below a flowstone. The excavation of the second pit, GE-II, started in 2009, and is located slightly closer to the ancient entrance of the cave, and currently has a total of 3 LUs identified below the flowstone. The LUs in each pit are numbered independently, according to their ordering from top to bottom, and do not indicate a correlation of levels across excavation areas. The description of the LUs was conducted in previous works (Arsuaga et al., 2017).

The archaeological-palaeontological remains are consistent with the sequence being deposited during the Upper Pleistocene, which is confirmed by U-series ages of ~14 ka and ~53 ka obtained for the flowstone or stalagmitic floor covering the sediment sequences (Marquet, 1988; Vernot et al., 2021). Single-grain OSL dating of sedimentary quartz grains indicate that LU4 to LU1 in pit GE-I were deposited between 112 ± 7 ka and 80 ± 5 ka, while LU2 to LU1 in GE-II were deposited between 79 ± 5 and 70 ± 5 ka (Demuro et al., 2019). ESR/U-series dating of mammal teeth (Moreno et al., 2022) has resulted in slightly more variable ages (i.e., a younger age of 92 ± 6 ka for the base of GE-I and an older age of 115 ± 18 ka for the base of GE-II), but overall, both studies indicate that the internal sediment sequence at Galería de las Estatuas was deposited during MIS 5 and the beginning of MIS 4.

3. Methodology

3.1. Optically stimulated luminescence (OSL) dating

Five single-grain OSL dating samples were collected in excavation pit GE-II of Galería de las Estatuas: one sample (GE18-1) from LU1, three samples (GE18-2, GE18-3 and GE22-3) from LU2, and one sample (GE22-2) from LU3 (Fig. S1). All samples were collected from cleaned exposure faces using opaque PVC tubes or by carefully scraping sediment into an opaque bag under subdued red LED illumination. After collection, samples were immediately sealed with light-proof plastic. Additional bulk sediment (approximately 500 g) was also collected from material directly surrounding each single-grain OSL sample for dosimetry and water content assessments.

Full details of the luminescence dating procedures employed in this study, including sample preparation, instrumentation, dose rate estimation, single-grain rejection criteria, and D_e measurement procedures, are provided in the Supplementary Information (S.I.). For consistency, we have adopted the same experimental conditions as those used in the original quartz single-grain OSL dating study of the site (Demuro et al., 2019). Unfortunately, the limited yields of coarse-grained K-feldspar in the Galería de las Estatuas deposits precludes undertaking complementary single-grain post-infrared infrared stimulated luminescence (pIR-IRSL) analyses for the samples considered here. Quartz grains were extracted under safe light conditions (600 or 630 nm LEDs, <0.15 $\mu W/cm^2$ power density at sample position) at the University of Adelaide using standard preparation procedures (e.g., Murray et al., 2021), including a 48% hydrofluoric acid etch (40 min) to remove the alpha-irradiated outer layers of the quartz extracts. Purified 212–250 μm quartz grains were manually loaded onto aluminium discs drilled with an array of 300 × 300 μm holes to ensure true single-grain resolution during equivalent dose (D_e) evaluation (Arnold et al., 2012a).

Individual D_e values were determined using the single-aliquot regenerative-dose (SAR) procedure (Murray and Wintle, 2000) shown in Table S2, which has yielded suitable multiple-grain aliquot and single-grain dose-recovery test results for sample GE18-3 (see Supplementary Information) and a closely related Galería de las Estatuas sample (GE16-1; see Supplementary Information of Demuro et al., 2019). Between 2000 and 3300 single-grain OSL D_e measurements were made for each sample (Table 1). Individual D_e values were excluded from the final age calculation if they did not satisfy a series of standard and widely tested quality-assurance criteria, as detailed in the Supplementary Information. Sensitivity-corrected dose-response curves were constructed using the first 0.09 s of each OSL stimulation after subtracting a mean background count obtained from the last 0.25 s of the signal (Fig. S2).

The environmental dose rates were estimated using a combination of *in situ* field gamma spectrometry and low-level beta counting, as described in Demuro et al. (2019), together with cosmic ray contributions (Prescott and Hutton, 1994), an assumed minor internal alpha dose rate (Bowler et al., 2003), beta-dose attenuation (Mejdahl, 1979; Brennan, 2003) and long-term water content (Aitken, 1985), as detailed in Table 1 and the S.I.

3.2. Study of the small mammal fossil remains

This study examines remains from all the lithostratigraphic units. We have analysed a total of 189 samples from both pits and different levels as shown in Table 2. In addition to the morphological characteristics a study by geometric morphometrics, described in the S.I., has been performed to improve the separation of *M. arvalis* from *M. agrestis,* as well as *T. lusitanicus* from *T. pyrenaicus*.

The morphological differentiation and taxonomic identifications of the Arvicolinae species have been carried out following the works of Chaline (1972), van der Meulen (1973), Brunet-Lecomte (1990) and Cuenca-Bescós and Morcillo-Amo (2022). In addition, we have used the

Table 1
Dose rate data, single-grain OSL equivalent doses and ages for the Galería de las Estatuas samples from pit GE-II.

Sample	Unit	Grain size (μm)	Water content (%)[a]	Environmental dose rate (Gy/ka)					Equivalent dose (D_e) data				Age (ka) [f,j]
				Beta dose rate[b]	Gamma dose rate [c]	Cosmic dose rate [d]	Internal dose rate [e]	Total dose rate [f]	No. of grains [g]	Overdis-persion (%) [h]	Age Model [i]	D_e (Gy) [f]	
GE18-1	LU1	212–250	25.6	1.27 ± 0.06	0.42 ± 0.02	0.02 ± 0.01	0.03 ± 0.01	1.75 ± 0.09	157/2000	24 ± 3	CAM	121.7 ± 3.4	69.7 ± 4.3
GE18-2	LU2 upper	212–250	13.9	1.02 ± 0.05	0.48 ± 0.02	0.02 ± 0.01	0.03 ± 0.01	1.56 ± 0.07	186/3000	34 ± 3	MAM-3	128.8 ± 12.3	82.8 ± 9.0
GE18-3	LU2 middle	212–250	28.6	1.03 ± 0.05	0.50 ± 0.02	0.02 ± 0.01	0.03 ± 0.01	1.57 ± 0.08	208/2100	28 ± 2	CAM	135.9 ± 3.5	86.4 ± 5.3
GE22-3	LU2 lower	212–250	12.6	1.35 ± 0.07	0.50 ± 0.02	0.02 ± 0.01	0.03 ± 0.01	1.90 ± 0.10	174/3300	27 ± 3	CAM	174.2 ± 5.1	91.8 ± 5.8
GE22-2	LU3	212–250	18.6	1.12 ± 0.06	0.59 ± 0.02	0.02 ± 0.01	0.03 ± 0.01	1.76 ± 0.09	156/2400	27 ± 3	CAM	166.8 ± 4.9	95.0 ± 5.7

[a] Present-day water content expressed as % of dry mass of mineral fraction, with an assigned 1σ uncertainty of ±10%. For sample GE22-3 the water content used for calculation of the gamma dose rate was the same as sample GE18-3 (see footnote c).

[b] Beta dose rates were calculated using a Risø GM-25-5 low-level beta counter (Bøtter-Jensen and Mejdahl, 1988), after making allowance for beta dose attenuation due to grain-size effects and HF etching (Mejdahl, 1979; Brennan, 2003). Radionuclide concentrations and specific activities of beta counting standards have been converted to dose rates using the conversion factors given in Guérin et al. (2011).

[c] Gamma dose rates were calculated from *in situ* measurements made at each sample position with a NaI:Tl detector using the 'energy windows' method detailed in Arnold et al. (2012b) and Duval and Arnold (2013). Radionuclide concentrations and specific activities of gamma spectrometry calibration materials, and K, U, Th concentrations determined from the field gamma-ray spectra have been converted to dose rates using the conversion factors given in Guérin et al. (2011). The *in situ* gamma dose rate of sample GE22-3 was as measured for sample GE18-3 given the very close proximity of these two samples (sample GE18-3 was located 7 cm above GE22-3; See Fig. S1).

[d] Cosmic-ray dose rates were calculated according to Prescott and Hutton (1994) and assigned a relative 1σ uncertainty of ±10%.

[e] The assumed internal alpha + beta dose rate for quartz, with an assigned relative 1σ uncertainty of ±30%, is based on intrinsic ^{238}U and ^{232}Th contents published by Mejdahl (1987), Bowler et al. (2003) Jacobs et al. (2006), Pawley et al. (2008) and Lewis et al. (2020), and an a-value of 0.04 ± 0.01 (Rees-Jones, 1995; Rees-Jones and Tite, 1997). Intrinsic radionuclide concentrations and specific activities have been converted to dose rates using the conversion factors given in Guérin et al. (2011), making allowance for beta dose attenuation due to grain-size effects (Mejdahl, 1979).

[f] Mean ± total uncertainty (68% confidence interval), calculated as the quadratic sum of the random and systematic uncertainties.

[g] Number of D_e measurements that passed the SAR rejection criteria and were used for D_e determination/total number of D_e values analysed.

[h] The relative spread in the D_e dataset beyond that associated with the measurement uncertainties for individual D_e values.

[i] CAM = central age model; MAM-3 = 3-parameter minimum age model (Galbraith et al., 1999).

[j] Total uncertainty includes a systematic component of ±2% associated with laboratory beta-source calibration.

Table 2
Distribution of the studied species by lithostratigraphic unit (LU), and diversity in species (S) for pits GE-I and GE-II at Galería de las Estatuas.

GE-I	*Arvicola sapidus*	*Microtus arvalis*	*Microtus agrestis*	*Microtus arvalis/ agrestis*	*Terricola lusitanicus*	*Terricola pyrenaicus*	*Pliomys lenki*	*Iberomys cabrerae*	Species (S)	Samples
LU1	–	2	3	–	–	–	–	–	2	3
LU1/2	–	19	21	1	–	–	2	–	3	12
LU2	6	21	30	10	1	–	2	–	5	17
LU2/3	–	21	33	11	3	–	–	–	3	10
LU3	4	128	156	34	17	3	3	–	6	47
LU3/4	–	4	4	–	2	1	1	–	5	3
LU4	2	11	10	15	3	2	–	–	5	6
LU4/5	–	1	3	–	1	–	–	–	3	1
LU5	–	1	1	–	–	–	1	–	3	2
Total GE-I	12	208	261	71	27	6	9	–		101
GE-II										
LU1	1	51	32	14	–	–	4	–	4	11
LU1/2	–	7	4	1	–	–	–	–	2	4
LU2	3	193	165	51	17	3	10	1	7	63
LU2/3	–	–	1	–	–	–	–	–	1	1
LU3	5	16	16	10	3	–	–	–	4	9
Total GE-II	9	267	218	76	20	3	14	1		88

nomenclature indicated by Abramson and Lissovsky (2012) and Petrova et al. (2014). In these papers, the subgenera of the genus *Microtus* are elevated to the genus systematic level: *Alexandromys*, *Terricola* and *Iberomys*. We have not adopted the classification of *Agricola* as a genus when referring to *M. agrestis* because we have not been able to verify if the specimens indicated by the authors correspond to the same species found GE.

We have studied the Arvicolinae species present in GE. According to Arsuaga et al. (2017) these genera are: *Microtus* (*M. arvalis* and *M. agrestis*), *Alexandromys* (*A. oeconomus*), *Iberomys* (*I. cabrerae*), *Terricola* (*T. lusitanicus* and *T. pyrenaicus*), traditionally included in *Microtus sensu lato* (*Microtus s.l.*), *Arvicola sapidus* and *Pliomys* (*P. lenki*). The paleontological systematics of this species can be found in the S.I.

The studied Galería de las Estatuas samples are from sediments collected during the 2008–2019 excavation seasons, which were washed and sieved following the small mammal study common methodology

(Cuenca-Bescós and Morcillo-Amo, 2022). Taxonomic classification was performed on the lower first molars (m1) of the Arvicolinae species. These anatomical elements are used in paleontological systematics for the diagnosis of the fossils of Arvicolinae species because they are one of the most diagnostic, abundant and well-preserved fossils remains.

Following identification, the Arvicolinae species have been used to infer environmental and climatic, as well as temperature, variations through the deposit of GE. For temperature reconstruction we have used the methodology of Montuire et al. (1997), who correlate the temperature of different present-day areas with the number of Arvicolinae species present. Apart from *P. lenki*, all of the studied species have extant representatives, thus allowing us to make an approximation of the habitat and climate of the past. For this reason, we have used the information provided by Palomo et al. (2007) on the present characteristic habitats of these small mammals in the Iberian Peninsula. Only *P. lenki* is extinct, though it could be related to the extant species *Dinaromys bogdanovy* (Chaline et al., 1999), and may be associated with a similar habitat of the living Martino or Balkans vole.

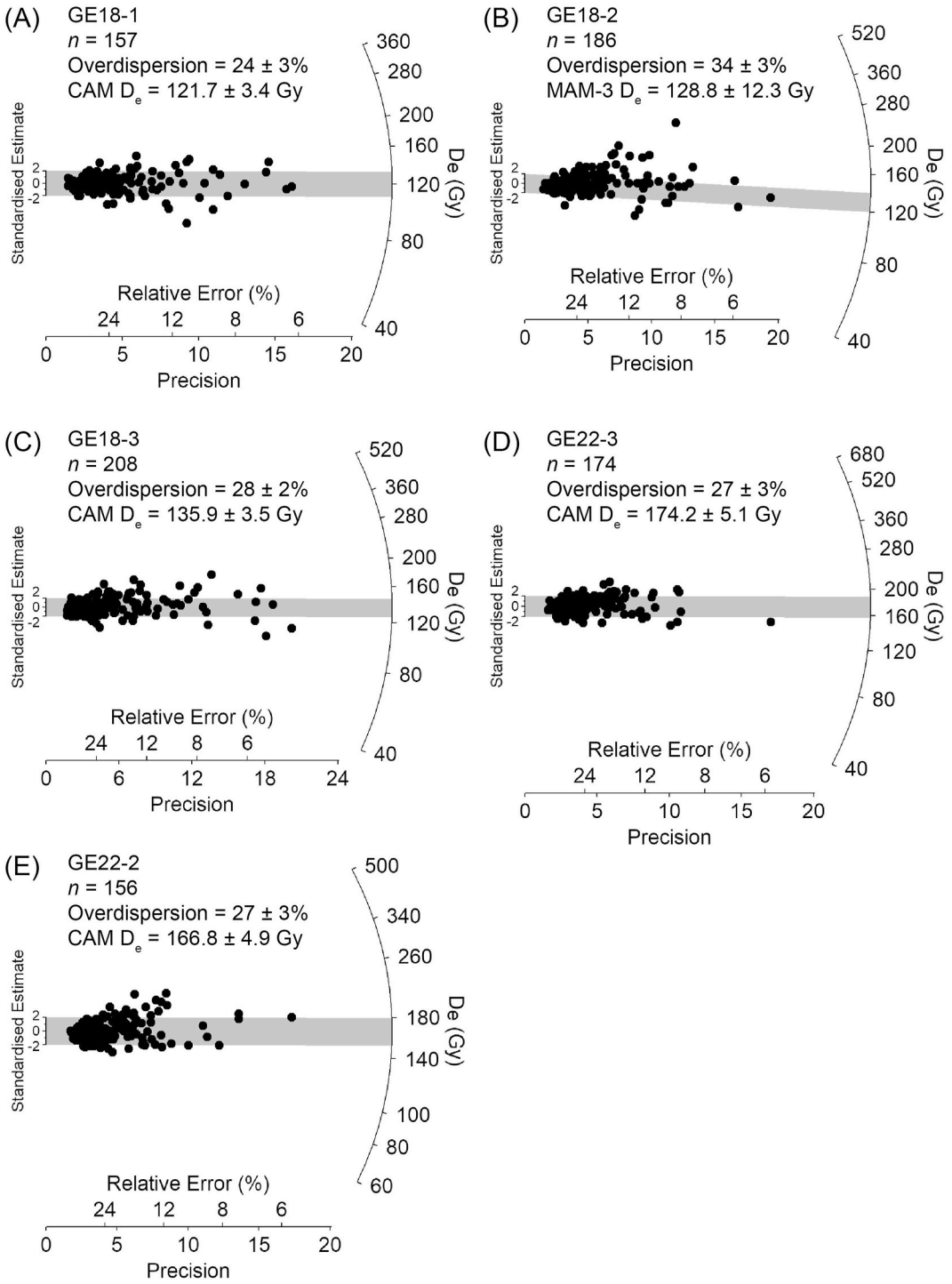

Fig. 2. Radial plots showing the single-grain OSL D_e distributions obtained for samples (A) GE18-1, (B) GE18-2, (C) GE18-3, (D) GE22-3 and (E) GE22-2 (D_e errors are shown at 1σ). For each sample, the grey band is centred on the central or minimum age model D_e value used to calculate the mean burial dose. Corresponding Abanico plots are shown in Fig. S3.

4. Results

4.1. Optically stimulated luminescence (OSL) dating

A summary of the environmental dose rates, single-grain D_e values and final ages obtained for the five OSL dating samples from GE pit GE-II is shown in Table 1. Between 5 and 10% of measured grains were considered suitable for OSL dating purposes after application of the SAR quality assurance criteria, with the majority of measured quartz grains (60–67%) rejected from final age estimations because they exhibited weak or no OSL signals (Table S3). Representative OSL dose-response and decay curve for grains that passed the quality assurance criteria are shown in Fig. S2. Consistent with the findings of Demuro et al. (2019), the apparent characteristic saturation dose (apparent D_0) values of these accepted grains (calculated using a single saturating exponential dose-response curve fit) are high enough to enable finite D_e determination over the observed burial dose ranges for these samples; hence the single-grain burial dose estimates are not considered to have been negatively affected by dose saturation. This is reinforced by the dose-recovery test results for sample GE18-3 (see Supplementary Information for details), which confirms the suitability of the SAR procedure for reliably measuring mean doses of 170 Gy. i.e., equivalent to the highest mean natural dose range encountered in this study.

Fig. 2 shows the single-grain OSL D_e distributions of grains that passed the SAR quality assurance criteria. Samples GE18-1, GE18-3, GE22-3 and GE22-2 exhibit similar D_e distributions characterised by relatively low scatter, with overdispersion values between 24 ± 3% and 28 ± 2%. These D_e distributions are not considered to be significantly positively skewed according to the criterion outlined by Arnold and Roberts (2009) (see Table S4) and the scatter observed is closely distributed around the average D_e value (Fig. 2; Table S4). In accordance with these favourable D_e characteristics, the final ages of GE18-1 and GE18-3 have been calculated using their weighted mean D_e values, which have been determined using the central age model (CAM) (Table 1). The application of the 3-parameter and 4-parameter minimum age models (MAM-3 and MAM-4) did not result in a significantly better fit than the CAM (according to the maximum log likelihood (L_{max}) scores shown in Table S4), which supports our age model selection for these four samples.

In contrast, the D_e distribution of sample GE18-2 is characterised by moderate-to-high dose dispersion (i.e., a distinct proportion of D_e values lying outside of the weighted mean (CAM) burial dose 2σ ranges), a prominent D_e cluster around ~130 Gy, and a tail of higher D_e values reaching up to ~430 Gy (Fig. 2B). The overdispersion value for this sample (34 ± 3%) is higher than that reported previously for well-bleached and unmixed single-grain OSL D_e datasets from Galería de las Estatuas (average = 24 ± 1%; $n = 7$ samples; see Table 1 of Demuro et al., 2019), as well as the average overdispersion of 20 ± 1% reported for ideal samples by Arnold and Roberts (2009). This overdispersion value is also significantly higher than the overdispersion value of 10 ± 5% obtained for the single-grain dose recovery test of sample GE16-1 (Supplementary Information of Demuro et al., 2019). Though the distribution is only moderately positively skewed (i.e., not statistically significant at the 95% C.I.; Table S4), application of the maximum log likelihood (L_{max}) test (Arnold et al., 2009) indicates that the MAM-3 of Galbraith et al. (1999) is statistically favoured over the CAM for this D_e dataset (Table S4). These various D_e characteristics suggest that dose dispersion originating from field-related sources has exerted a minor to moderate influence on sample GE18-2. Given the potentially complex transportation and depositional processes that can take place within shallow karst cavities (e.g., Arnold et al., 2022; Jankowski et al., 2016; Prideaux et al., 2010; Priya et al., 2022), we consider the enhanced D_e scatter for GE18 as most likely originating from insufficient resetting of OSL signals for the high tail grain populations, or syn-depositional mixing of pre-existing cave sediments with predominantly well-bleached, externally derived quartz grains during their initial transportation within the cave system. Consequently, the final D_e value of GE18-2 has been calculated using the MAM-3, which has been shown to be suitable for isolating the most recently and completely sub-populations of grains in partially bleached or syn-depositionally mixed karst samples (e.g. Arnold et al., 2019; Benito-Calvo et al., 2020; Zilhão et al., 2020; Daura et al., 2021; David et al., 2021; Ruiz et al., 2021).

The final ages obtained for the Galería de las Estatuas samples are shown in Table 1. The uppermost sample, GE18-1, collected from LU1 of pit GEII, produces an age of 69.7 ± 4.3 ka, while the two samples from upper LU2 and middle LU2 (GE18-2 and GE18-3, respectively) yield corresponding ages of 82.8 ± 9.0 ka and 86.4 ± 5.3 ka. These ages are in agreement with those obtained by Demuro et al. (2019) for the same levels, though in the former study the samples were collected from the opposing face of the GE-II excavation. For samples GE22-3 and GE22-2, which were collected from lower LU2 and LU3, respectively, the corresponding single-grain OSL ages are 91.8 ± 5.8 ka and 95.0 ± 5.7 ka. The combined set of ages confirm that LU1 and LU2 of GE-II were most likely deposited within late MIS 5, but the depositional sequence may have extended into early MIS 4 when taking into consideration the OSL dating 2σ uncertainty ranges.

4.2. Microfaunal analyses

4.2.1. Identification of the species

A total of 1201 specimens were identified from the 189 samples studied, and these were classified into seven species: *A. sapidus, M. arvalis, M. agrestis, T. lusitanicus, T. pyrenaicus, P. lenki* and *I. cabrerae*. (Fig. 3). Arsuaga et al. (2017) identified *Alexandromys oeconomus*, though in this study we see that it is absent. The identified specimen is in fact a poorly preserved m1 of *M. agrestis* with a broken AC, thus making accurate classification difficult.

4.2.2. Distribution of species in the Galería de las Estatuas sequence

Both LU3 in GE-I and LU2 in GE-II display a significant increase in the number of individuals per species compared to the underlying units, accounting for more than 50% of the identified m1s (>70% in GE-II) and number of species (Table 2 and Fig. 4). However, the upper part of LU2 in GE-II exhibits a decrease in the number of species and identified m1s. These two LUs also have a higher frequency of *Terricola* in their middle and lower parts. In both pits, *M. arvalis* and *M. agrestis* are the only Arvicolinae that appear constantly through the sequence. *A. sapidus* is also observed in almost all the LUs, only absent in LU5 of GE-I and LU1 of GE-II probably due to the small amount of sample studied from these levels, and not necessarily related to the climatic conditions at the time of deposition.

In GE-I we observe a progressive increase in the total number of individuals from LU4 at the base to the upper half of LU3, followed by a progressive decrease during LU2. *P. lenki* is present in all levels of the pit. In contrast, the *Terricola* species are only observed up until the lower half of LU2, except for *T. pyrenaicus*, which is only present in LU3 and LU4 of this pit. In the GE-II sequence we observe a similar progressive increase in the number of individuals and biodiversity from LU3 to LU2. *P. lenki* is only observed in LU1 and LU2. The only individual of *I. cabrerae* at this site is found in LU2, along with both species of the genus *Terricola*. The last appearance of *T. pyrenaicus* in this pit occurs just below the appearance of *I. cabrerae* (Fig. 4).

4.2.3. Climatic interpretations

Examination of the quantitative distribution of Arvicolinae species through the stratigraphic sequence of Galería de las Estatuas allows us to infer the climatic variations that took place during sediment deposition. We have deduced the mean temperature corresponding with each stratigraphic level following the approach outlined in Montuire et al. (1997) (Table 2). In GE-I there was a general increase in the mean temperature from LU4 (1 °C to 15 °C) to LU1 (9 °C to 20 °C), but with the

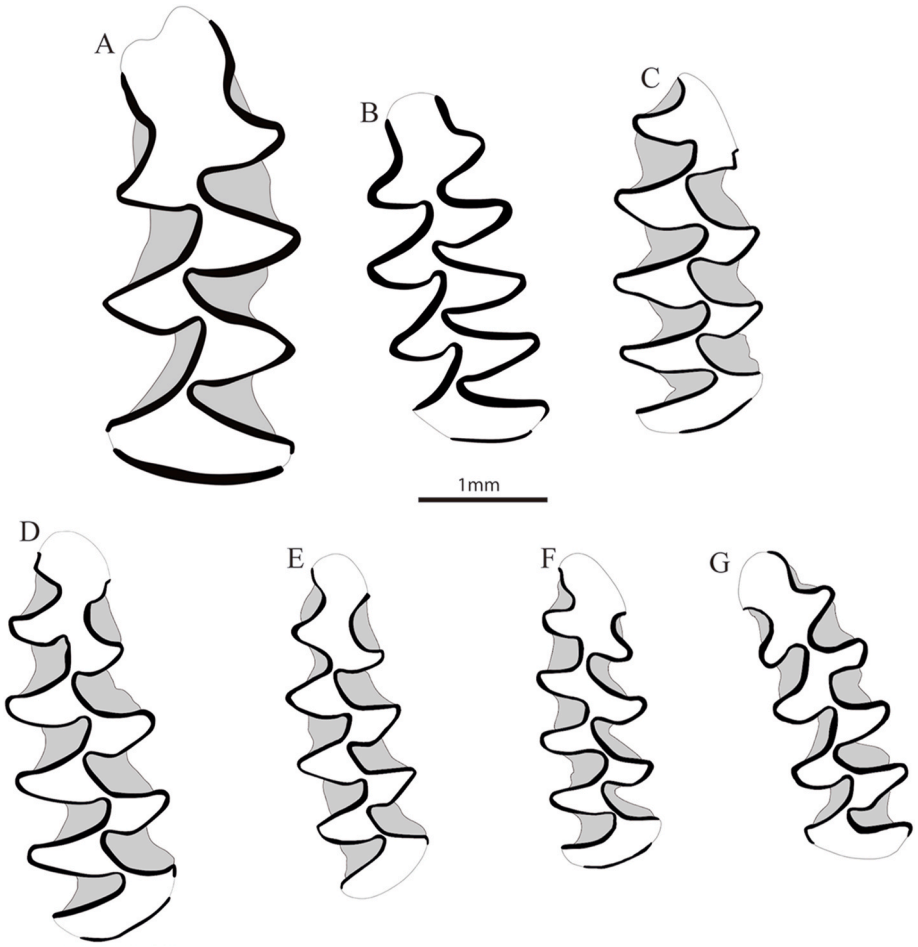

Fig. 3. Illustrations of the m1 of the Arvicolinae species from Galería de las Estatuas site. A: *Arvicola sapidus* (GE-I, square: N21, z: 260–270, LU3); B: *Pliomys lenki* (GE-II, square: E31, z: 180–190, LU2); C: *Iberomys cabrerae* (GE-II, square: D34, z: 160–170, LU2); D: *Microtus agrestis* (GE-I, square: N29, z:?, LU1); E: *Microtus arvalis* (GE-I, square: N31, z: 250–260, LU3); F *Terricola lusitanicus* (GE-II, square: D34, z: 130–144, LU2); G: *Terricola pyrenaicus* (GE-I, square: M31, z: 300–310, LU4). Grey areas are the cement of the entrant angles; black lines the enamel wall, and the white fields, surrounded by the enamel, the dentine of the first lower molars, m1. Observe the lack of cement in the entrants of *Pliomys lenki*.

lowest temperatures estimated to occur in LU3 (-4 °C to 11 °C). We infer a similar pattern for GE-II, though note that LU3 of this pit is still under excavation. A similar mean temperature range is inferred for LU3 and LU1 in GE-II (5 °C to 18 °C), while LU2 displays the lowest mean temperatures from the site (-8 °C to 7 °C). It should be noted that the latter temperature range would only be valid for the middle to lower part of LU2 in GE-II as the decrease in number of species observed for the upper part of LU2 indicates higher temperatures that are in closer agreement with those observed in LU1.

The arvicolines from Galería de las Estatuas are associated with open meadows, with differences regarding their climate regime, mean temperatures, and environmental stability. *Dinaromys bogdanovi* is present in habitats from mountain areas, with a rocky stable substrate, and require climatic conditions to be stable over longer periods of times (Kryštufek, 2018), thus, this is the inferred habitat for *Pliomys lenki*. Fossils of *P. lenki* are present in open environments, and their numbers decrease when there is a predominance of forest (Marquet, 1988; Cuenca-Bescós et al., 2010). *A. sapidus* occupy areas near permanent water bodies, like riverbanks with abundant riverine vegetation. The two described *Microtus* species, *M. arvalis* and *M. agrestis*, currently inhabit a wide variety of habitats, and thus exhibit opportunistic behaviours. Both are typical of open and humid landscapes, with an Atlantic type climatic regime, and constant herbaceous cover, as well as near young forest areas. The two species of the genus *Terricola* inhabit open and humid environments and are indicative of more stable and warmer climatic conditions. *T. lusitanicus* specifically is characteristic of areas with an Atlantic type of climatic regime. Meanwhile, *T. pyrenaicus,* is observed in mountain areas where the mean annual temperatures are around 15/16 °C. Lastly, *I. cabrerae* is only present in zones with a Mediterranean-type climatic regime characterised by warm and humid conditions, high ground water levels and constant herbaceous cover.

5. Discussion

5.1. Climate reconstructions for the Galería de las Estatuas sequence

Arsuaga et al. (2017) presented the first palynological study and approximation of the small mammal association of the Galería de las Estatuas reconstructing the climatic conditions prevailing during the formation of the sedimentary sequence. The climatic changes observed by the authors are generally in concordance with the distribution of Arvicolinae species identified throughout the sequence. Our new study includes data from LU5 of GE-I and LU3 of GE-II.

The site is chronologically constrained to MIS 5, with GE-II also spanning the beginning of MIS 4 (Demuro et al., 2019; Moreno et al., 2022). Specifically, LU3 and LU4 of GE-I most likely corresponds to MIS 5.4, a cold sub-stadial of the MIS 5, while the upper half of LU2 in GE-I most likely corresponds to MIS 5.1, a warm sub-stadial (Demuro et al., 2019). The new OSL ages presented here suggests that LU3 of GE-II likely accumulated during MIS 5.3, LU2 accumulated during MIS

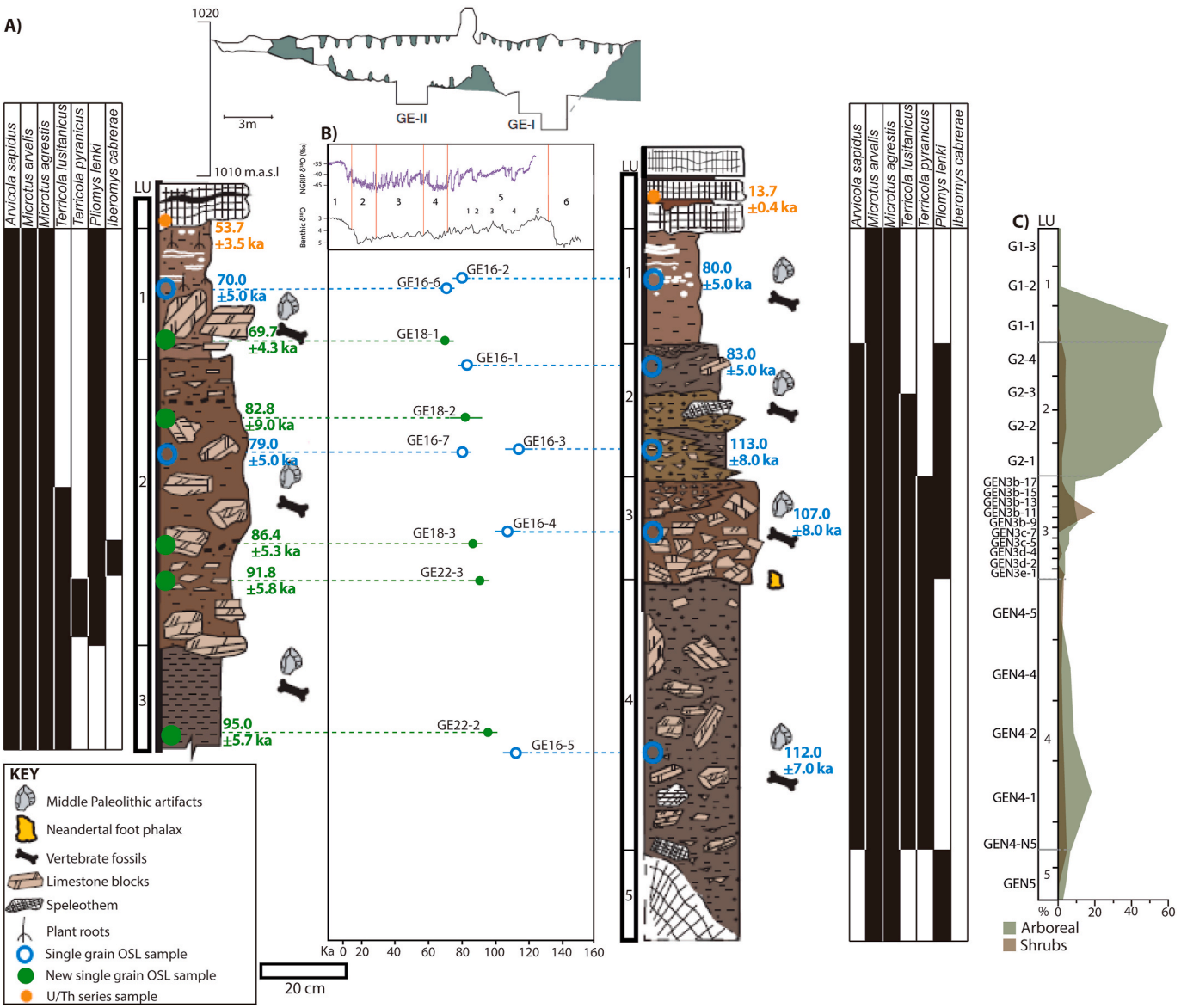

Fig. 4. **A)** Cross section of the Galería de las Estatuas site and stratigraphy, modified from Vernot et al. (2021). We add here the distribution of the Arvicolinae species and the new OSL samples. **B)** Single grain OSL ages (and associated 1σ errors) of both pits modified from Demuro et al. (2019), plotted with the Marine Isotopic Stage (MIS) (Lisiecki and Raymo, 2005), and the $\delta^{18}O$ isotope curves for the last glacial cycle (NGRIP and Intermediate North Atlantic records; Andersen et al., 2004; Lisiecki and Stern, 2016). **C)** Interpretative diagram of the palynological sequence of GE-I, representing the percentage of arboreal and shrubs dominance, modified from Arsuaga et al. (2017).

5.2–5.1, and LU1 during MIS 5.1 to possibly the beginning of MIS 4, thus confirming the previous OSL dating results obtained for the GE-II upper levels (Demuro et al., 2019).

What follows is an account of our interpretations regarding the climatic conditions at Galería de las Estatuas reached using the data from small mammals and palynological associations from Arsuaga et al. (2017), the chronological data from Demuro et al. (2019) and the new data presented of this study.

In the GE-I sequence, our results point to a change in climate conditions from LU4 to LU2. These observations are in general accordance with the palynological study, although there are some discrepancies in LU2 and LU3 regarding the predominance of forested areas. In particular, the palynological data identified a larger proportion of arboreal pollen, in which Pinus is predominant though it does not reach the threshold to be considered a closed forest during LU2, which prevailed from the base of LU1. However, the small mammal association is inconsistent with the predominance of forest zones during LU2 because Terricola and Microtus species, as well as the bat taxa *Myotis myotis/blythii*) are associated with open landscapes, whilst species typical of forest environments are absent. There is a significant development of forest areas in LU3, with higher biodiversity and presence of typical inhabitants of forest areas such as *Eliomys quercinus* and *Apodemus* sp. pointing to better environmental conditions than in other levels.

The abundance of open habitat species in LU2 of GE-I indicates the predominance of herbaceous and shrub meadows. The presence of P. *lenki* in LU2 and LU3 is remarkable because it is not compatible with widespread development of forested areas. LU3 and LU4 contain species that are associated with both warm temperatures, *T. lusitanicus, Hystrix vinogradovi*, and colder temperate climatic conditions, *T. pyrenaicus*, *Marmota marmota*, which is in accordance with its dating to MIS 5.4 (Fig. 4), one of the cold sub-stadial of the MIS 5. Between LU3 and LU4, Vernot et al. (2021) observed genetic differences between the Neandertal populations that inhabited Galería de las Estatuas by analysing aDNA recovered from sediments. These differences were interpreted as a

population replacement occurring roughly 100 ka ago. Whether this replacement was intrinsic (i.e., due to stochastic population dynamics) or extrinsic (climate change) is currently unknown. Differences in the proportion of mesophilous taxa has been detected between LU4 and LU3 in the Galería de las Estatuas sequence (Arsuaga et al., 2017) but the small mammal faunal assemblages are very similar between the end of LU4 and the start of LU3.

The absence of *A. oeconomus* does not modify the initial palaeoecological interpretations that LU3 is characterised by high humidity and the presence of water bodies nearby, because there is a record of other species that are attributable to this type of environment, such as *A. sapidus*. The disappearance of cold climate species in the upper levels is indicative of an increase in mean temperatures. This interpretation would also be in concordance with the dating of the upper part of LU2 in GE-I to MIS 5.1, which also follows a sedimentary hiatus, as indicated by the OSL dating of Demuro et al. (2019). The high number of *Terricola* individuals at the bottom of LU2 in GE-I, and the similarities in the biodiversity between LU2 and LU3, support with the OSL age obtained for the bottom of LU2 (113 ± 8 ka), which is in better agreement with the age obtained for underlying LU3 (107 ± 8 ka) than with the upper part of LU2 (83 ± 5 ka). After the hiatus in LU2, *T. lusitanicus* disappear in the upper part of this level, and no further important changes are observed in the other Arvicolinae. The absence of *Terricola* during LU1 could indicate a deterioration of climatic conditions in this level, with increased development of open landscapes. However, the small number of samples from this level could equally be attributable to geological factors, such as the progressive closing of the cave entrance, rather than being a genuine indicator of changing palaeoecological conditions.

In GE-II there is a progressive improvement in climatic conditions, persisting during the lower part of LU2, where more than the 70% of the *Terricola* individuals from this pit are identified. Moreover, LU2 is the only level of GE-II that preserves *T. pyrenaicus* and contains the only individual of *I. cabrerae* identified at the site thus far (Fig. 4). *I. cabrerae* is located at the lower-middle part of LU2, after the last appearance of *T. pyrenaicus*. The presence of the Cabrera vole is indicative of a marked Mediterranean type of climatic regime, which is in contrast with the presence of *T. pyrenaicus*, typical of an Atlantic climatic regime and lower temperatures. The new OSL dating results for sample GE18-3 indicate that the lower-middle part of LU2, where we observe *I. cabrerae,* could correspond within MIS 5.1, thus being consistent with the warmer climatic conditions. On the other hand, the other OSL age obtained for the bottom half of this level (GE22-3), where *T. pyrenaicus* is present, may correlate to MIS 5.2, a cold substage. Note that these correlations are tentative given the relatively large uncertainties (~6.5%) associated with the OSL ages.

Furthermore, LU2 has species that reflect higher humidity and the presence of water bodies near the cave *(A. sapidus* and *C. fiber*). Therefore, LU2 could be characterised as representing a period of significant climatic variations. In addition, there are forested areas nearby in LU2, based on the presence of *Apodemus* sp. and *Eliomys quercinus*. However, the predominance of species more characteristic of open landscapes (e.g., *Microtus, Terricola, I. cabrerae, Myotis myotis* and *P. lenki*) in the lower half of LU2 could indicate that forests were a relatively minor habitat component throughout most of this level and were perhaps restricted to small patches. The absence of Mediterranean species in LU1, and the presence of other species such as *P. lenki, M. arvalis* and *M. agrestis,* could mark a deterioration of climatic conditions, characterised by the dominance of open meadows and an Atlantic control regime, which could correspond with the beginning of MIS 4.

5.2. Comparison between the GE-I and GE-II pits

Arsuaga et al. (2017) observed climatic and palynological similarities between LU2s of both pits, whereas the OSL dating results of Demuro et al. (2019) suggest closer temporal correlations between LU2 and the bottom of LU1 of GE-I with the upper part of LU2 of GE-II. Our palaeoecological results shows that the bottom part of LU2 at GE-II is more similar, in terms of climatic conditions and biodiversity, to LU3 of GE-I. This similarity is most remarkable over the uppermost few centimetres of LU3 in GE-I and the lowermost few centimetres of LU2 in GE-II (Table 2). In addition, both levels also record the presence of *T. pyrenaicus*, absent in the overlying levels of both pits. The OSL dating studies thus far (i.e., Demuro et al., 2019 and this study) have not targeted the base of LU2 in GE-II. However, the age of 95.0 ± 5.7 ka for the underlying LU3 in GE-II indicates that both LU3 and the base of LU2 in GE-II were likely formed after the deposition of LU3 and lower part of LU2 in GE-I, which are dated to 107.0 ± 8.0 ka and 113 ± 8.0 ka, respectively (Demuro et al., 2019, Fig. 4). Again, there are some caveats with these temporal correlations across the two pits because the associated uncertainty ranges of the OSL ages preclude precise comparisons.

The lower half of the GE-I sequence (levels LU4, LU3 and the bottom of LU2) have been OSL dated to MIS 5.4, which is consistent with the climatic conditions of these levels being colder than those of the overlying levels of the sequence. The age obtained for the bottom half of LU2 in GE-II (91.8 ± 5.8 ka) could correspond with MIS 5.2, making these deposits younger than the corresponding LU2 levels of GE-I, but with similar climatic conditions; thus, both sets of sequences could represent two cold sub-stages within MIS 5. In contrast, the upper part of the LU2 deposits in GE-I and GE-II exhibit similarities in their climatic conditions inferred from the small mammal associations, their species biodiversity, and their corresponding OSL dating results (both those presented here and in Demuro et al., 2019), which indicate the upper LU2 deposits likely formed within MIS 5.1.

Taking into consideration previous studies of GE, and the distribution of species obtained in the current study, it is also probable that the bottom of LU1 in GE-I experienced similar climatic conditions to that of the upper part of LU2 in both pits. When comparing both LU1 deposits, we observe the presence of *P. lenki* in LU1 of GE-II, which could indicate more restricted development of forest areas in comparison with LU1 of GE-I, where this species was not observed (Fig. 4). However, the absence of this species in LU1 of GE-I could be a consequence of the smaller number of samples studied.

There are currently no dating results available for the lowermost level described in pit GE-I (LU5), so the chronological interpretations of these deposits remain limited. The Arvicolinae assemblage observed for LU5 is composed by *P. lenki, M. arvalis* and *M. agrestis* (Table 2). Interestingly, this association of species is not observed elsewhere at GE, though this could be due to the smaller number of samples studied from LU5.

6. Conclusions

The detailed examination of the Arvicolinae record at the Galería de las Estatuas, and comparison with available chronological data and previous palynological climatic reconstructions, have enabled insights into the climatic changes, at the level of identified sub-stadial changes that took place during the formation of GE, and the period of its Neandertal occupation.

GE experienced a shift from somewhat unfavourable climate conditions at the start of LU4 (GE-I), characterised by more arid and colder temperate conditions, with an Atlantic type of climate regime, towards warmer, humid, and more stable climatic conditions (albeit retaining relatively cool temperatures) during LU4 of GE-I and LU3 of GE-II. The surroundings of the cave would have been dominated by open meadows, as indicated by the presence of *M. agrestis, M. arvalis*, *Terricola* and *P. lenki.* The apex of these more favourable climatic conditions is observed from LU3 to the base or lower half of LU2 in GE-I, as well as at the base of LU2 in GE-II. The association of these small mammal faunas are indicative of cold to temperate conditions and the OSL dating results suggest these units were most likely deposited during MIS 5.4 or MIS 5.2 (for GE-I and GE-II, respectively). The presence of *I. cabrerae* in the lower-middle part of LU2 (GE-II) indicates a transition to warmer and

more humid climatic conditions, potentially corresponding with MIS 5.1. The upper parts of the LU2 (within MIS 5.1) deposits in both pits and the disappearance of *I. cabrerae* and *Terricola,* indicate a slightly decrease in environmental stability. The uppermost deposits of both sequences (LU1s) record a significant worsening of climatic conditions, characterised by drier environments, stronger Atlantic influences and the predominance of open landscapes, most likely corresponding to the start of MIS 4. We conclude that at least two marked climatic changes can be identified at each pit of Galería de las Estatuas, from MIS 5.4 through to the beginning of MIS 4.

Declaration of competing interest

The authors declare that they have no known competing financial interests or personal relationships that could have appeared to influence the work reported in this paper.

Data availability

Data will be made available on request.

Acknowledgments

This study has been possible thanks to the work of the Galería de las Estatuas excavation and research team. Supported by the Spanish Ministerio de Ciencia e Innovación (Project PID2021–122355NB-C31, MCIN/AEI/10.13039/501100011033/FEDER, UE). MPAI and GCB work is founded by the Government of Aragón-ERDF (Group E18: Aragosaurus:Recursos Geológicos y Paleoambientales). MPAI has a grant from Ministerio de Universidades (FPU20/02031). AGO is supported by Ramón y Cajal fellowship (RYC-2017-22558). MD was supported by Australian Research Council (ARC) Future Fellowship FT200100816 and ARC Discovery Early Career Researcher Award DE160100743. Fieldwork is supported by the Junta de Castilla y León and Fundación Atapuerca.

Appendix A. Supplementary data

Supplementary data to this article can be found online at https://doi.org/10.1016/j.quascirev.2024.108939.

References

Abramson, N.I., Lissovsky, A.A., 2012. Subfamily arvicolinae. In: Pavlinov, I.Y., Lissovsky, A.A. (Eds.), En: the Mammals of Russia: a Taxonomic and Geographic Reference, Archive of the Zoological Museum of MSU, vol. 52. KMK Scientific Press, Moscow, pp. 220–276.

Aitken, M.J., 1985. Thermoluminescence Dating. Academic Press, London, p. 359.

Andersen, K.K., Azuma, N., Barnola, J.-M., Bigler, M., Biscaye, P., Caillon, N., Chappellaz, J., Clausen, H.B., Dahl-Jensen, D., Fischer, H., Flückiger, J., Fritzsche, D., Fujii, Y., Goto-Azuma, K., Grønvold, K., Gundestrup, N.S., Hansson, M., Huber, C., Hvidberg, C.S., Johnsen, S.J., Jonsell, U., Jouze, J., Kipfstuh, S., Landais, A., Leuenberger, M., Lorrain, R., Masson-Delmotte, V., Miller, H., Motoyama, H., Narita, H., Popp, T., Rasmussen, S.O., Raynaud, D., Rothlisberger, R., Ruth, U., Samyn, D., Schwander, J., Shoji, H., Siggard-Andersen, M.-L., Steffensen, J. P., Stocker, T., Sveinbjörnsdóttir, A.E., Svensson, A., Takata, M., Tison, J.-L., Thorsteinsson, Th, Watanabe, O., Wilhelms, F., White, & J.W.C., 2004. High-resolution record of Northern hemisphere climate extending into the last interglacial period. Nature 431, 147–151.

Arnold, L.J., Roberts, R.G., Galbraith, R.F., DeLong, S.B., 2009. A revised burial dose estimation procedure for optical dating of young and modern-age sediments. Quat. Geochronol. 4, 306–325. https://doi.org/10.1016/j.quageo.2009.02.017.

Arnold, L.J., Roberts, R.G., 2009. Stochastic modelling of multi-grain equivalent dose (De) distributions: implications for OSL dating of sediment mixtures. Quat. Geochronol. 4, 204–230. https://doi.org/10.1016/j.quageo.2008.12.001.

Arnold, L.J., Demuro, M., Navazo Ruiz, M., 2012a. Empirical insights into multi-grain averaging effects from 'pseudo' single-grain OSL measurements. Radiat. Meas. 47, 652–658. https://doi.org/10.1016/j.radmeas.2012.02.005.

Arnold, L.J., Duval, M., Falguères, C., Bahain, J.-J., Demuro, M., 2012b. Portable gamma spectrometry with cerium-doped lanthanum bromide scintillators: suitability assessments for luminescence and electron spin dating applications. Radiat. Meas. 47, 6–18. https://doi.org/10.1016/j.radmeas.2011.09.001.

Arnold, L.J., Demuro, M., Parés, J.M., Arsuaga, J.L., Aranburu, A., De Castro, J.M.B., Carbonell, E., 2014. Luminescence dating and palaeomagnetic age constraint on hominins from Sima de los Huesos, Atapuerca, Spain. J. Hum. Evol. 67, 85–107. https://doi.org/10.1016/j.jhevol.2013.12.001.

Arnold, L.J., Demuro, M., Spooner, N.A., Prideaux, G.J., Mcdowell, M.C., Camens, A.B., Reed, E.H., Parés, J.M., Arsuaga, J.L., Bermúdez de Castro, J.M., Carbonell, E., 2019. Single-grain TT-OSL bleaching characteristics: insights from modern analogues and OSL dating comparisons. Quat. Geochronol. 49, 45–51. https://doi.org/10.1016/j.quageo.2018.01.004.

Arnold, L.J., Demuro, M., Power, R., Priya, Duval, M., Guilarte, V., Weij, R., Woodhead, J., White, L., Bourne, S., Reed, E.H., 2022. Examining sediment infill dynamics at Naracoorte Cave megafauna sites using multiple luminescence dating signals. Quat. Geochronol. 70, 101301 https://doi.org/10.1016/j.quageo.2022.101301.

Arsuaga, J.L., Martínez, I., Arnold, L.J., Aramburu, A., Gracia-Téllez, A., Sharp, W.D., Quam, R.M., Falguères, C., Pantoja-Pérez, A., Bischoff, J., PozaRey, E., Parés, J.M., Carretero, J.M., Demuro, M., Lorenzo, C., Sala, N., Martinóm-Torres, M., García, N., AlcázardeVelasco, A., Cuenca-Bescós, G., Gómez-Olivencia, A., Moreno, D., Pablos, A., Shen, C.-C., Rodríguez, L., Ortega, A.I., García, R., Bonmatí, A., Bermúdez de Castro, J.M., Carbonell, E., 2014. Neandertal roots: Cranial and chronological evidence from Sima de los Huesos. Science 344, 1358–1363. https://doi.org/10.1126/science.1253958.

Arsuaga, J.L., Carretero, J.M., Lorenzo, C., Gómez-Olivencia, A., Pablos, A., Rodríguez, L., Garcia-González, R., Bonattí, A., Quam, R.M., PantojaPérez, A., Martínez, I., Aranburu, A., Gracia-Télles, A., Poza-Rey, E.M., Sala, N., Garcia, N., Alcazar deVelasco, A., Cuenca-Bescós, G., Bérmudez de Castro, J.M., Carbonell, E., 2015. Postcranial morphology ofthe Middle Pleistocene humans from Sima de los Huesos, Spain. Proc. Natl. Acad. Sci. USA 112 (37), 11524–11529. https://doi.org/10.1073/pnas.1514828112.

Arsuaga, J., Gómez-Olivencia, A., Sala, N., Martínez-Pillado, V., Pablos, A., Bonmatí, A., Pantoja-Pérez, A., Lira-Garrido, J., Alcázar de Velasco, A., Ortega, A.I., Cuenca-Bescós, G., García, N., Aranburu, A., Ruiz-Zapata, B., Gil-García, M.J., Rodríguez-Álvarez, X.P., Ollé, A., Mosquera, M., 2017. Evidence of paleoecological changes and Mousterian occupations at the Galería de las Estatuas site, Sierra de Atapuerca, northern Iberian plateau, Spain. Quaternary Research 88 (2), 345–367. https://doi.org/10.1017/qua.2017.46.

Bañuls-Cardona, S., López-García, J.M., Morales Hidalgo, J.I., Cuenca-Bescós, G., Vergès, J.M., 2017. Lateglacial to Late Holocene palaeoclimatic and palaeoenvironmental reconstruction of El Mirador cave (Sierra de Atapuerca, Burgos, Spain) using the small-mammal assemblages. Palaeogeogr. Palaeoclimatol. Palaeoecol. 471, 71–81. https://doi.org/10.1016/j.palaeo.2017.01.019.

Benito-Calvo, A., Arnold, L.J., Mora, R., Martínez-Moreno, J., Demuro, M., 2020. Reconstructing mousterian landscapes in the southeastern pyrenees (roca dels bous site, pre-pyrenees ranges, Spain). Quaternary Research 97, 167–186. https://doi.org/10.1017/qua.2020.29.

Bennàsar Serra, M.L., Cáceres, I., Cuenca-Bescós, G., 2016. Paleoecological and microenvironmental aspects of the first European hominids inferred from the taphonomy of small mammals (Sima del Elefante, Sierra de Atapuerca, Spain). Comptes Rendus Palevol 15 (6), 635–646. https://doi.org/10.1016/j.crpv.2015.07.006.

Berger, G.W., Pérez-González, A., Carbonell, E., Arsuaga, J.L., De Castro, J.B., Ku, T., 2008. Luminescence chronology of cave sediments at the Atapuerca paleoanthropological site, Spain. J. Hum. Evol. 55 (2), 300–311. https://doi.org/10.1016/j.jhevol.2008.02.012.

Bermúdez de Castro, J.M., Arsuaga, J.L., Carbonell, E., Rosas, A., Martínez, I., Mosquera, M., 1997. A hominid from the Lower Pleistocene of Atapuerca. Spain: possible ancestor to neandertals and modern humans. Science 276, 1392–1395. https://doi.org/10.1126/science.276.5317.1392.

Blois, J.L., McGuire, J.L., Hadly, E.A., 2010. Small mammal diversity lossin response to late-Pleistocene climatic change. Nature 465, 771–774. https://doi.org/10.1038/nature09077.

Brennan, B.J., 2003. Beta doses to spherical grains. Radiat. Meas. 37, 299–303. https://doi.org/10.1016/S1350-4487(03)00011-8.

Brunet-Lecomte, P., 1990. Evolution morphologique de la premiere molaire inferieure des campagnols Souterrains d'Europe (Arvicolidae, Rodentia). Z. Säugetierkunde 55, 371–382.

Bøtter-Jensen, L., Mejdhal, V., 1988. Assessment of beta dose-rate using a GM multicounter system. Nucl. Tracks Radiat. Meas. 14, 187–191. https://doi.org/10.1016/1359-0189(88)90062-3.

Bowler, J.M., Johnston, H., Olley, J.M., Prescott, J.R., Roberts, R.G., Shawcross, W., Spooner, N.A., 2003. New ages for human occupation and climate change at Lake Mungo, Australia. Nature 421, 837–840. https://doi.org/10.1038/nature01383.

Carbonell, E., De Castro, J.M.B., Parés, J.M., Pérez-González, A., Bescós, G.C., Ollé, A., Mosquera, M., Huguet, R., Van Der Made, J., Rosas, A., Sala, R., Vallverdú, J., Garcia, N., Granger, D.E., Martinón-Torres, M., Rodriguez, X.P., Stock, G.M., Vergès, J.M., Allué, E., Arsuaga, J.L., 2008. The first hominin of Europe. Nature 452 (7186), 465–469. https://doi.org/10.1038/nature06815.

Chaline, J., 1972. Les rongeurs du Pleistocène moyen et supèrieur de France. Cahiers de Paléontologie CNRS, pp. 1–410.

Chaline, J., Brunet-Lecomte, P., Montuire, S., Viriot, L., Courant, F., 1999. Anatomy of the arvicoline radiation (Rodentia): palaeogeographical, palaeoecological history and evolutionary data. Ann. Zool. Fenn. 36 (4), 239–267. http://www.jstor.org/stable/23735732.

Cuenca-Bescós, G., Straus, L.G., González Morales, M.R., García Pimienta, J.C., 2008. Paleoclima y paisaje del final del cuaternario en Cantabria: los pequeños mamíferos

del Mirón (Ramales de la Victoria). Rev. Esp. Palaontol. 23, 91–126. https://doi.org/10.7203/sjp.23.1.20398.

Cuenca-Bescós, G., Straus, L.G., García-Pimienta, J.C., González Morales, M., López-García, J.M., 2010. Faunal turnover in the late Pleistocene in cantabria. The extinction of Pliomys lenki (Rodentia mammalia). Quaternary Internacional 212, 129–136. https://doi.org/10.1016/j.quaint.2009.06.006.X.

Cuenca-Bescós, G., Melero-Rubio, M., Rofes, J., Martínez, I., Arsuaga, J.L., Blain, H.A., López-García, J.M., Carbonell, E., Bermudez de Castro, J.M., 2011. The Early-Middle Pleistocene environmental and climatic change and the human expansion in Western Europe: a case study with small vertebrates (Gran Dolina, Atapuerca, Spain). J. Hum. Evol. 60 (4), 481–491. https://doi.org/10.1016/j.jhevol.2010.04.002.

Cuenca-Bescós, G., Morcillo-Amo, A., 2022. *Roedores, edades y paisajes en el Cuaternario de la Península Ibérica*. Prames. Guías de la naturaleza, p. 416, 978-84-8321-537-1.

David, B., Arnold, L.J., Delannoy, J.-J., Fresløv, J., Urwin, C., Petchey, F., McDowell, M. C., Mullett, R., Land, G., Mialanes, J., 2021. Late survival of megafauna refuted for Cloggs Cave, SE Australia: implications for the Australian Late Pleistocene megafauna extinction debate. Quat. Sci. Rev. 253, 106781 https://doi.org/10.1016/j.quascirev.2020.106781.

Daura, J., Sanz, M., Demuro, M., Arnold, L.J., Costa, A.M., Moreno, J., da Conceição Freitas, M., Lopes, V., Égüez, N., Hoffmann, D.L., Benson, A., Cabanes, D., García-Targa, J., Fullola, J.M., 2021. A new chronological framework and site formation history for Cova del Gegant (Barcelona): Implications for Neanderthal and Anatomically Modern Human occupation of NE Iberian Peninsula. Quat. Sci. Rev. 270, 107141 https://doi.org/10.1016/j.quascirev.2021.107141.

Demuro, M., Arnold, L.J., Aranburu, A., Gómez-Olivencia, A., Arsuaga, J.L., 2019. Single-grain OSL dating of the Middle Palaeolithic site of Galería de las Estatuas, Atapuerca (Burgos, Spain). Quat. Geochronol. 49, 254–261. https://doi.org/10.1016/j.quageo.2018.02.006.

Demuro, M., Arnold, L.J., Parés, J.M., Aranburu, A., Huguet, R., Vallverdú, J., Arsuaga, J. L., De Castro, J.M.B., Carbonell, E., 2022. Extended-range luminescence chronologies for the Middle Pleistocene units at the Sima del Elefante archaeological site (Sierra de Atapuerca, Burgos, Spain). Quat. Geochronol. 71, 101318 https://doi.org/10.1016/j.quageo.2022.101318.

Duval, M., Arnold, L.J., 2013. Field gamma dose-rate assessment in natural sedimentary contexts using LaBr3(Ce) and NaI(Tl) probes: a comparison between the "threshold" and "windows" techniques. Appl. Radiat. Isot. 74, 36–45. https://doi.org/10.1016/j.apradiso.2012.12.006.

Duval, M., Arnold, L.J., Demuro, M., Parés, J.M., Lozano, I.C., Carbonell, E., De Castro, J. M.B., 2022. New chronological constraints for the lowermost stratigraphic unit of Atapuerca Gran Dolina (Burgos, N Spain). Quat. Geochronol. 71, 101292 https://doi.org/10.1016/j.quageo.2022.101292.

Galán, J., Bañuls-Cardona, S., Cuenca-Bescós, G., Vergès, J.M., 2022. Understanding the biogeography of Western European bats: the latest Pleistocene to Middle Holocene assemblage of El Mirador site (Sierra de Atapuerca, Spain). Hist. Biol. 1–15. https://doi.org/10.1080/08912963.2022.2107430.

Galbraith, R.F., Roberts, R.G., Laslett, G.M., Yoshida, H., Olley, J.M., 1999. Optical dating of single and multiple grains of quartz from Jinmium rock shelter, northern Australia: Part I, experimental design and statistical models. Archaeometry 41, 339364. https://doi.org/10.1111/j.1475-4754.1999.tb00987.x.

Guérin, G., Mercier, M., Adamiec, G., 2011. Dose-rate conversion factors: update. Ancient TL 29, 5–8.

Jacobs, Z., Duller, G.A.T., Wintle, A.G., Henshilwood, C.S., 2006. Extending the chronology of deposits at Blombos Cave, South Africa, back to 140 ka using optical dating of single and multiple grains of quartz. J. Hum. Evol. 51, 255–273. https://doi.org/10.1016/j.jhevol.2006.03.007.

Jankowski, N.R., Gully, G.A., Jacobs, Z., Roberts, R.G., Prideaux, G.J., 2016. A late Quaternary vertebrate deposit in Kudjal Yolgah Cave, south-western Australia: refining regional late Pleistocene extinctions. J. Quat. Sci. 31, 538–550. https://doi.org/10.1002/jqs.2877.

Kryštufek, B., 2018. Dinaromys bogdanovi. The IUCN Red List of Threatened Species 2018: e.T6607A97220104. https://dx.doi.org/10.2305/IUCN.UK.2018-1.RLTS.T6607A97220104.en.

Lewis, R.J., Tibby, J., Arnold, L.J., Barr, C., Marshall, J., McGregor, G.B., Gadd, P., Yokoyama, Y., 2020. Insights into subtropical Australian aridity from welsby Lagoon, north Stradbroke Island, over the past 80,000 years. Quat. Sci. Rev. 234, 106262 https://doi.org/10.1016/j.quascirev.2020.106262.

Lisiecki, L.E., Raymo, M.E., 2005. A Pliocene-Pleistocene stack of 57 globally distributed benthic δ18O records. Paleoceanography 20. https://doi.org/10.1029/2004PA001071. PA 1003.

Lisiecki, L.E., Stern, J.V., 2016. Regional and global benthic δ18O stacks for the last glacial cycle. Paleoceanography 31, 1364–1394. https://doi.org/10.1002/2016PA003002.

López-García, J., Blain, H., Cuenca-Bescós, G., Ruiz-Zapata, M., Dorado-Valiño, M., Gil-García, M., Valdeolmillos, A., Ortega, A., Carretero, J., Arsuaga, J., de Castro, J., Carbonell, E., 2010. Palaeoenvironmental and palaeoclimatic reconstruction of the Latest Pleistocene of El Portalón Site, Sierra de Atapuerca, northwestern Spain. Palaeogeogr. Palaeoclimatol. Palaeoecol. 292 (3–4), 453–464. https://doi.org/10.1016/j.palaeo.2010.04.006.

López-García, J.M., Berto, C., Cuenca-Bescós, G., Galindo-Pellicena, M.A., Luzi, E., Berto, C., Lebreton, L., Desclaux, E., 2021. Rodents as indicators of climatic conditions in which hominins lived during the late Middle Pleistocene in southwestern Mediterranean. J. Hum. Evol. https://doi.org/10.1016/j.jhevol.2020.102911.

Marquet, J.C., 1988. L'Homme de Neanderthal et son environnement dans la moitié ouest de la France d'aprés les rongeurs. Etudes et Recherche Archéologique de l'Université de Liège 29, 105–110.

Mejdahl, V., 1979. Thermoluminescence dating: beta-dose attenuation in quartz grains. Archaeometry 21, 61–72.

Mejdahl, V., 1987. Internal radioactivity in quartz and feldspar grains. Ancient TL 5, 10–17.

Montuire, S., Michaux, J., Legendre, S., Aguilar, J.P., 1997. Rodents and climate. 1. A model for estimating past temperatures using arvicolids (Mammalia: Rodentia). Palaeogeogr. Palaeoclimatol. Palaeoecol. 128 (1–4), 187–206. https://doi.org/10.1016/s0031-0182(96)00038-7.

Moreno, D., Ortega, A.I., Falguères, C., Shao, Q., Tombret, O., Gómez-Olivencia, A., Aranburu, A., Trompier, F., Bermúdez De Castro, J.M., Carbonell, E., Arsuaga, J.L., 2022. ESR/U-series chronology of the Neanderthal occupation layers at Galería de las Estatuas (Sierra de Atapuerca, Spain). Quat. Geochronol. 72, 101342 https://doi.org/10.1016/j.quageo.2022.101342.

Murray, A.S., Wintle, A., 2000. Luminescence dating of quartz using an improved single-aliquot regenerative-dose protocol. Radiat. Meas. 32, 57–73. https://doi.org/10.1016/S1350-4487(99)00253-X.

Murray, A., Arnold, L.J., Buylaert, J.-P., Guérin, G., Qin, J., Singhvi, A.K., Smedley, R., Thomsen, K.J., 2021. Optically stimulated luminescence dating using quartz. Nature Reviews Methods Primers 1, 72. https://doi.org/10.1038/s43586-021-00068-5.

Ortega, A.I., 2009. La evolución geomorfológica del karst de la Sierra de Atapuerca (Burgos) y su relación con los yacimientos pleistocenos que contiene. In: Tesis Doctoral, vol. 624p. Universidad de Burgos.

Ortega, A.I., Benito-Calvo, A., Pérez-González, A., Martín-Merino, M.Á., Pérez-Martínez, R., Parés, J.M., Aramburu, A., Arsuaga, J.L., De Castro, J.M.B., Carbonell, E., 2013. Evolution of multilevel caves in the Sierra de Atapuerca (Burgos, Spain) and its relation to human occupation. Geomorphology 196, 122–137. https://doi.org/10.1016/j.geomorph.2012.05.031.

Palomo, L.J., Gisbert, J., Blanco, J.C., 2007. Atlas y Libro Rojo de los Mamíferos Terrestres de España. Dirección General para la Biodiversidad-SECEM-SECEMU, p. 588. Madrid.

Pablos, A., Gómez-Olivencia, A., Arsuaga, J.L., 2019. A Neandertal foot phalanx from the Galería de las Estatuas site (Sierra de Atapuerca, Spain). Am. J. Phys. Anthropol. 168 (1), 222–228. https://doi.org/10.1002/ajpa.23729.

Pawley, S.M., Bailey, R.M., Rose, J., Moorlock, B.S.P., Hamblin, R.J.O., Booth, S.J., Lee, J.R., 2008. Age limits on Middle Pleistocene glacial sediments from OSL dating, north Norfolk, UK. Quat. Sci. Rev. 27, 1363–1377. https://doi.org/10.1016/j.quascirev.2008.02.013.

Petrova, T.V., Zakharov, E.S., Samiya, R., Abramson, N.I., 2014. Phylogeography of the narrow-headed vole *Lasiopodomys* (*Stenocranius) gregalis* (Cricetidae, Rodentia) inferred from mitochondrial cytochrome b sequences: an echo of Pleistocene prosperity. JZSER 53 (2), 97–108. https://doi.org/10.1111/jzs.12082.

Prescott, J.R., Hutton, J.T., 1994. Cosmic ray contributions to dose rates for luminescence and ESR dating: large depths and long-term time variations. Radiat. Meas. 23, 497–500. https://doi.org/10.1016/1350-4487(94)90086-8.

Priya, Arnold L.J., Guilarte, V., Duval, M., Demuro, M., Weij, R., Reed, E.H., 2022. ESR and OSL dating of fossil-bearing deposits from Naracoorte Cave Complex palaeontological sites, south Australia. Quat. Geochronol. 69, 101270 https://doi.org/10.1016/j.quageo.2022.101270.

Prideaux, G.J., Gully, G.A., Couzens, A.M.C., Ayliffe, L.K., Jankowski, N.R., Jacobs, Z., Roberts, R.G., Hellstrom, J.C., Gagan, M.K., Hatcher, L.M., 2010. Timing and dynamics of Late Pleistocene mammal extinctions in southwestern Australia. Proc. Natl. Acad. Sci. USA 107, 22157–22162. https://doi.org/10.1073/pnas.1011073107.

Rees-Jones, J., 1995. Optical dating of young sediments using fine-grain quartz. Ancient TL 13, 9–14.

Rees-Jones, J., Tite, M.S., 1997. Optical dating results for British archaeological sediments. Archaeometry 39, 177–187. https://doi.org/10.1111/j.1475-4754.1997.tb00797.x.

Ruiz, M.N., Benito-Calvo, A., Alonso-Alcalde, R., Alonso, P., de la Fuente, H., Santamaría, M., Santamaría, C., Álvarez-Vena, A., Arnold, L.J., Iriarte-Chiapusso, M. J., 2021. Late Neanderthal subsistence strategies and cultural traditions in the northern Iberia Peninsula: insights from prado vargas, Burgos, Spain. Quat. Sci. Rev. 254, 106795 https://doi.org/10.1016/j.quascirev.2021.106795.

Van der Meulen, A.J., 1973. Middle Pleistocene smaller mammals from the monte peglia, (Orvieto, Italy) with special reference to the phylogeny of Microtus (arvicolinae, Rodentia). Quaternaria XVII, 144p. Roma.

Vernot, B., Zavala, E.I., Gómez-Olivencia, A., Jacobs, Z., Slon, V., Mafessoni, F., Romagné, F., Pearson, A., Petr, M., Sala, N., Pablos, A., Aranburu, A., de Castro, J.M. B., Carbonell, E., Li, B., Krajcarz, M.T., Krivoshapkin, A.I., Kolobova, K.A., Kozlikin, M.B., Meyer, M., 2021. Unearthing Neanderthal population history using nuclear and mitochondrial DNA from cave sediments. Science 372 (6542). https://doi.org/10.1126/science.abf1667.

Zilhão, J., Angelucci, D.E., Igreja, M.A., Arnold, L., Badal, E., Callapez, P., Cardoso, J.L., D'Errico, F., Daura, J., Demuro, M., 2020. Last interglacial Iberian neandertals as Fisher-hunter-gatherers. Science 367. https://doi.org/10.1126/science.aaz7943.